LIMNOLOGY and OCEANOGRAPHY

ASLO

Limnol. Oceanogr. 69, 2024, 2830–2845

doi: 10.1002/lno.12711

A 7-yr spatial time series resolves the island mass effect and associated shifts in picocyanobacteria abundances near O'ahu, Hawai'i

Christina M. Comfort [1*] **Chris Ostrander** [2,3] **Craig E. Nelson** [1,4,5] **David M. Karl** [1,4] **Margaret A. McManus** [1]

[1]Department of Oceanography, University of Hawai'i at Mānoa, Honolulu, Hawai'i, USA
[2]School of Ocean and Earth Science and Technology, University of Hawai'i at Mānoa, Honolulu, Hawai'i, USA
[3]Marine Technology Society, Washington, DC, USA
[4]Daniel K. Inouye Center for Microbial Oceanography: Research and Education, Honolulu, Hawai'i, USA
[5]Hawai'i Sea Grant, University of Hawai'i, Honolulu, Hawai'i, USA

Abstract

Islands in oligotrophic oceans act as local sources of nutrients. These nutrients originate from land and from deep oceanic nutrients introduced to the photic zone by tides, currents, and internal waves interacting with island bathymetry. These processes create the island mass effect (IME), in which increased chlorophyll *a* (Chl *a*) is found near islands compared to oceanic waters. The IME has been described via satellite observations, but the effects on phytoplankton community structure are not well documented. From 2013 to 2020, chlorophyll, nutrient, and picoplankton samples were collected from multiple depths on quarterly cruises at two sites south of O'ahu, Hawai'i. *Prochlorococcus*, *Synechococcus*, picoeukaryotes, and heterotrophic bacteria were enumerated using flow cytometry. We compared nearshore results to Sta. ALOHA, 100 km from O'ahu. Consistent with the expected IME, Chl *a* concentrations were significantly enhanced at both nearshore sites compared to Sta. ALOHA. *Prochlorococcus* concentrations increased with greater distance from shore, particularly below 50 m; mixed layer concentrations of *Synechococcus* and picoeukaryotes significantly decreased with greater distance from shore, as did concentrations of nitrate and phosphate below the mixed layer. Heterotrophic bacteria concentrations did not show a spatial trend. Carbon-based biomass estimates of the picoplankton population indicated that the IME-associated Chl *a* increases near the island are likely driven by larger phytoplankton classes. This study describes the IME-associated shift in the picophytoplankton community distribution, which has implications for nutrient cycling, food web dynamics and fisheries in oligotrophic island ecosystems, and adds to the understanding of spatial heterogeneity in carbon fixation in the ocean.

*Correspondence: ccomfort@hawaii.edu

Additional Supporting Information may be found in the online version of this article.

Author Contribution Statement: CMC: Writing – original draft preparation; Writing – review and editing; Investigation; Data curation; Formal analysis; Visualization. CEO: Conceptualization; Funding acquisition; Supervision; Methodology; Writing – review and editing. CEN: Formal analysis; Methodology; Writing – review and editing. DMK: Conceptualization; Funding acquisition; Supervision; Methodology; Writing – review and editing. MAM: Conceptualization; Funding acquisition; Supervision; Methodology; Formal analysis; Writing – review and editing.

The island mass effect

In oligotrophic oceans, nutrients and primary productivity are low compared to upwelling regions and continental shelf ecosystems, but hot spots of productivity are found near islands and atolls, which therefore support higher levels of zooplankton and fishery biomass. The increased productivity found near islands and atolls is called the island mass effect (IME) (Dandonneau and Charpy 1985). The IME has been well-documented in terms of chlorophyll *a* (Chl *a*) and estimated phytoplankton biomass increases near islands (Gove et al. 2016; Messié et al. 2022), but picoplankton community composition and IME-related shifts are less well understood. In this study we investigate the shifts in the picoplankton community from nearshore to oceanic waters over a 7-yr time

series near O'ahu, Hawai'i, and explore relationships to factors such as nutrient availability and water column stability.

The IME has been observed via shipboard observations since the mid-20th century near Hawai'i (Doty and Oguri 1956; Gilmartin and Revelante 1974). Satellite Chl *a* observations have allowed this effect to be documented throughout oligotrophic ocean basins (Gove et al. 2016; Messié et al. 2022). This localized biomass enhancement is caused by higher levels of inorganic nutrients in nearshore island water compared to nutrient-limited oceanic waters nearby, and this increase in nutrients can be driven by both oceanographic processes and land-based inputs. Oceanographic processes include the interaction of tides and internal waves with island bathymetry, which creates turbulent mixing that introduces deeper, more nutrient-rich waters to the mixed layer, and shoaling of the pycnocline (De Falco et al. 2022). Also, the impingement of large-scale currents on island bathymetry can drive IME via upward doming of isopycnals in the lee of the current (Signorini et al. 1999; De Falco et al. 2022) and formation of eddies that create localized upwelling (e.g., Arístegui et al. 1994; Seki et al. 2001). Islands can cause alterations in wind patterns that drive deeper mixing (Hernández-León 1991) and cause eddies to form which can upwell nutrients to the surface and cause increases in productivity (Hernández-León 1991; Arístegui et al. 1994). Coral reef organisms can alter the nutrient biogeochemistry of local reef water (Nelson et al. 2023) which may then be advected to backreef and nearshore waters (Hench et al. 2008; Nelson et al. 2011; Leichter et al. 2013). Land-based inputs of nutrients can include human and animal waste, fertilizer from agricultural and landscaping applications, and iron-rich land inputs from soil. These inputs can enter the marine environment through surface waters such as streams and storm runoff (e.g., Laws et al. 1994; Lapointe and Bedford 2011) or submarine groundwater discharge (Moosdorf et al. 2015).

The IME is observed near-ubiquitously throughout the Pacific Ocean with varying levels of intensity at different islands (Messié et al. 2022). In a basin-scale survey of Pacific Islands, it was found that the IME enhances phytoplankton biomass by up to 85.6% over background conditions (Gove et al. 2016). In the Hawaiian islands, satellite imagery and in situ measurements indicated at least a 30% increase in Chl *a* near the islands compared to oceanic waters, which translates to an increase of over 1250 kg of total phytoplankton biomass across the Hawaiian island chain compared to nearby oceanic waters (Gove et al. 2016). Most studies of the IME include in situ and/or satellite measurements of Chl *a*, a proxy for phytoplankton biomass, but few studies have investigated the changes in plankton community composition and size structure from nearshore to open ocean (Gilmartin and Revelante 1974; Rissik et al. 1997), and researchers are just beginning to characterize spatial shifts in the picoplankton community due to the IME (e.g., Tucker et al. 2021; Comstock et al. 2022). A recent study using ocean-color-based "phenoclasses" found that the ratio of *Synechococcus* and nanoplankton increases in the IME relative to the smaller *Prochlorococcus* (Messié et al. 2022).

Picoplankton in oligotrophic oceans

The picophytoplankton *Prochlorococcus*, *Synechococcus*, and picoeukaryotes contribute a significant amount of the primary production in the North Pacific Subtropical Gyre (NPSG). *Prochlorococcus* is the smallest known photoautotroph (Chisholm et al. 1992) and due to its large geographic distribution (40°S to 40°N) and high-light and low-light adapted ecotypes that enable it to succeed in a wide variety of habitats and conditions, it is likely the most abundant primary producer in the world (Partensky et al. 1999a). Despite its very small size (0.5–0.7 μm), *Prochlorococcus* has been found to contribute over 50% of the chlorophyll and up to 82% of the primary production at Sta. ALOHA (Liu et al. 1997; Rii et al. 2016), a long-term monitoring station located 100 km north of O'ahu, Hawai'i. Due to its very high surface area: volume ratio, *Prochlorococcus* is successful in highly oligotrophic regions. Their nutrient needs also may be extremely low and they may be able to effectively scavenge nutrients from elements recycled by heterotrophic bacteria (Biller et al. 2015; Partensky et al. 1999a). *Prochlorococcus* have a depth range that extends into the nutricline, which is deeper than other picophytoplankton, but most strains do not have the capability to use nitrate as a nutrient source, instead relying on remineralized N sources such as ammonium and urea. Some low-light adapted *Prochlorococcus* strains are capable of metabolizing nitrite (Moore et al. 2002), and even fewer can metabolize nitrate (Berube et al. 2023).

Synechococcus is a distant second to *Prochlorococcus* in terms of abundance in the NPSG, but is nevertheless a very important component of the picoplankton community structure and overall primary productivity. In nearshore reef habitats of Pacific subtropical gyres, *Synechococcus* is highly enriched and the dominant phytoplankton (Comstock et al. 2022). Larger than *Prochlorococcus* with a size range of 0.8–1.5 μm, *Synechococcus* thrives in regions with more available nutrients, and can also tolerate colder temperature than *Prochlorococcus*; therefore, in more eutrophic and/or temperate habitats, *Synechococcus* can become numerically more dominant (Comstock et al. 2022; Partensky et al. 1999b). Due to its larger size, it still contributes a significant portion of primary productivity and chlorophyll at Sta. ALOHA. It has a smaller depth range than *Prochlorococcus* and is found below 100 m only in very low concentrations in the NPSG (Campbell and Vaulot 1993; Partensky et al. 1999b). Contrary to *Prochlorococcus*, most *Synechococcus* strains have the ability to use nitrate or nitrite as their sole source of N (Moore et al., 2002; Bird and Wyman, 2003).

Picoeukaryotes are a diverse group of photosynthetic protists which, despite lower abundances, also contribute

substantially to carbon fixation and productivity in the NPSG due to their larger size class (Pasulka et al. 2013). This group can typically use nitrate as a source of N, though they often preferentially take up ammonia (Rii et al., 2018). Heterotrophic bacteria are a crucial component of the picoplankton community structure as key drivers of biogeochemical processes such as nutrient recycling and remineralization. They are extremely abundant and contribute a substantial fraction of the picoplankton biomass (Jones et al. 1996; Pasulka et al. 2013).

The goal of this study is to observe how the abundance and community composition of picoplankton changes due to the IME on the leeward shore of O'ahu, Hawai'i as compared to the oligotrophic NPSG. Using shipboard observations and flow cytometry, the island mass effect near O'ahu, Hawai'i is quantified over an 7-yr sampling period and abundances of *Prochlorococcus*, *Synechococcus*, picoeukaryotes, and heterotrophic bacteria are compared from locations in a near-shore open embayment, on the island slope, and in the open ocean.

Materials and methods

Study site

Field observations for this study took place within and just outside of Māmala Bay, to the south of O'ahu, Hawai'i, with comparisons to Sta. ALOHA to the north of O'ahu (Fig. 1). The leeward south shore of O'ahu has spur-and-groove coral reefs followed by a slope, then a steep shelf at about 100 m deep, and then a gradual slope to deeper oceanic waters (Ruhe et al. 1965). The highly urbanized southern coast of O'ahu is a significant source of nutrient input to the coastal ocean (Ruhe et al. 1965; Laws et al. 1999; Whittier and El-Kadi 2009, 2014). Over a 7-yr period between 2013 and 2020, oceanographic measurements and picoplankton samples were collected on 30 research cruises from two sites: S1, 2 km south of Honolulu, O'ahu (21.2763°N, 157.8740°W) and 200 m deep; and S2, 6.5 km south of Honolulu, O'ahu (21.2233°N, 157.8649°W) and 550 m deep (Fig. 1).

The island of O'ahu shelters S1 from east-northeasterly trade winds, while S2 is outside Māmala Bay and far enough south that it is more exposed to the trade winds (Comfort et al. 2015). Typical weather conditions during sampling were calm with a few occurrences of strong winds and currents that occasionally hindered sampling at S2. We compared our data to the Hawai'i Ocean Time-series program data collected at Sta. ALOHA (S3). S3 is located 100 km north of Kahuku Point, O'ahu (22.75°N and 158.00°W) at a depth of 4800 m. S3 is an open-ocean site which is far enough from O'ahu that it is not within the spatial influence of the IME. These three sites provide an onshore–offshore sampling gradient.

Climatological data

Daily mean wind speed, wind direction, and total rain data from the NOAA Local Climatological Data (Honolulu Airport station) were examined for seasonality. Seasons were defined by the seasonal distinctions recognized in native Hawaiian culture: *kau*, May–October, and *ho'oilo*, November–April. Two-sample *t*-tests were used to determine significant seasonal differences in wind and/or rainfall.

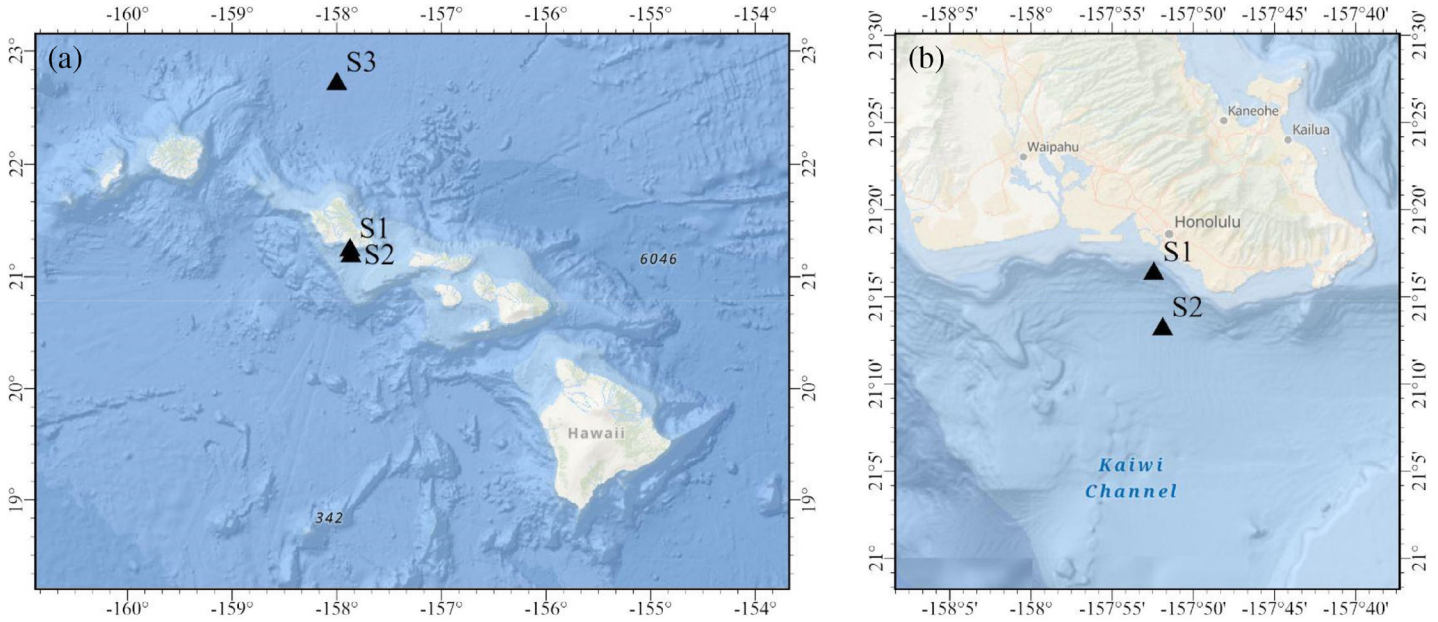

Fig. 1. Location of sampling sites near O'ahu, Hawai'i. S1 is 2 km from shore and 200 m deep. S2 is 6.5 km from shore and 550 m deep. S3 is Sta. ALOHA, 100 km from shore and 4800 m deep.

Field procedure

Seawater samples were collected in twelve 8 L Niskin® bottles on a sampling rosette alongside a conductivity–temperature–depth (CTD) sensor. The Seabird 911+ CTD was equipped with auxiliary sensors that provided profiles for dissolved oxygen (SBE43 Dissolved Oxygen Sensor), chlorophyll fluorescence and turbidity (WetLabs ECO-FLNT), and PAR (Biospherical Sensors). Samples from the 8 L Niskin® bottles were analyzed for dissolved inorganic nutrients (nitrate, phosphate, silicate), Chl *a*, and picoplankton cell abundances. Samples were collected from S1 at 5, 25, 45, 75, 100, 125, and 150 m, and S2 at 5, 25, 45, 75, 100, 150, 300, and 500 m. Chl *a* samples were collected into 150 mL opaque sample bottles. Nutrients were collected in 125 mL HDPE bottles and stored on dry ice until they could be transferred to a freezer for long-term storage. Each picoplankton sample was collected from the Niskin bottle with a 15 mL Falcon tube and then pipetted into 2 mL aliquots. Picoplankton samples were then preserved with 30 μL of 16% paraformaldehyde (0.24% total concentration), flash frozen in liquid nitrogen and stored at −80°C until analyzed.

Oceanographic data analysis

Nutrient samples were stored frozen at −20°C until analyzed, typically within 1 yr. Each sample was processed with a Seal Analytical model AAA segmented flow injection autoanalyzer (for details see Supporting Information). Chl *a* samples were filtered onto Whatman 25 mm GF/F glass fiber filters after each cruise. Studies have shown that 25 mm GF/F glass fiber filters are effective at capturing the smallest phototrophs (Chavez et al. 1995). The samples were then extracted and measured according to standard methods used by the Hawai'i Ocean Time-series (for details see Supporting Information). Satellite Chl *a* data from 2013 to 2020 at each site location were downloaded from NOAA's Coral Reef Watch ocean color database, which uses data from the Visible Infrared Imaging Radiometer Suite (VIIRS).

The deep chlorophyll maximum (DCM) was calculated for each season at each station using the Chl *a* profile from the ECO-FLNT fluorometer on the CTD package, and the DCM layer was identified as a depth range in each profile where the fluorescence signal ranged from 50% to 100% of the maximum signal surrounding the peak fluorescence reading. The 1% and 0.1% light levels were calculated using the observed light at 3 m depth as the "surface irradiance" and finding the depths that correspond to 1% and 0.1% of surface irradiance via a linear interpolation on log-transformed data.

The mixed layer depth (MLD) was determined by finding the depth at which the density was 0.125 kg m^{-3} greater than the surface density. The buoyancy frequency profile was calculated for each cast at a 2 m depth step:

$$N(z) = \left(\frac{g}{\rho}\frac{\delta\rho}{\delta z}\right)^{0.5}$$

where N is the buoyancy frequency, g is the acceleration due to gravity, ρ is the density, and z is the depth. Buoyancy frequency indicates the strength of the density gradient, and can therefore quantify the span of the pycnocline region or the density gradient at a specific feature such as the DCM (McManus et al., 2012). To examine the relationship of buoyancy frequency to the DCM, we calculated the average buoyancy frequency from 0 to 20 m, within the DCM layer, and below the DCM layer from 160 to 180 m at the shallow 2 km station (the deepest measurements available) and 240–260 m depth at the 6.5 and 100 km stations.

Cell counts and biomass estimates

Picoplankton cells were counted with a Cytopeia Influx Flow Cytometer following the methods of the Hawai'i Ocean Time-series. *Synechococcus* cells were distinguished based on their high orange fluorescence, then picoeukaryotes were located based on their high forward scatter, red, and orange fluorescence, and finally *Prochlorococcus* cells were identified based on their forward scatter vs. red fluorescence signal and refined using orange fluorescence vs. red fluorescence and side scattering (van den Engh et al. 2019; for detailed methods, see Supporting Information).

Heterotrophic bacteria were counted by first staining an aliquot of preserved sample with 5 μL of SYBR Green nucleic acid dye, and cells were identified based on green fluorescence and forward scatter. Cells were separated into high-scatter and low-scatter groups, presumably distinguished by high and low DNA contents (Silovic et al., 2018; Casey et al. 2019). The *Prochlorococcus* population was subtracted from the high-scatter cell group to arrive at the high-scatter heterotrophic bacteria population (Eric Shimabukuro, pers. comm; Casey et al. 2019). Examples of typical cytograms used to generate cell counts are shown in the Supporting Information Fig. S1.

The total carbon content for each picoplankton type was calculated using 25.7 fg cell^{-1} for *Prochlorococcus* (Casey et al. 2019), 50 fg cell^{-1} for *Synechococcus* (Rii et al. 2016), 453 fg cell^{-1} for picoeukaryotes (Rii et al. 2016), 5.9 fg cell^{-1} for low-scatter heterotrophs and 22.6 fg cell^{-1} for high-scatter heterotrophs (Casey et al. 2019) (for additional details see Supporting Information). Water column biomass estimates were found by integration of the observed data over depth using the trapezoid rule (e.g., Karl et al. 2022).

Sta. ALOHA (S3)

Data for Sta. ALOHA (S3) were obtained via the Hawai'i Ocean Time-series Data Organization & Graphical System application (HOT-DOGS; https://hahana.soest.hawaii.edu/hot/hot-dogs/). We used data from approximately monthly

cruises from 2013 to 2020 for the following parameters: picoplankton concentrations, dissolved inorganic nutrient concentrations, and Chl *a* concentration measured from bottle samples and instrumentation profiles.

Statistical analyses

We hypothesized that the IME would manifest as chemical and microbiological concentration gradients from nearshore to open ocean stations that vary with depth and season. To test these explicit hypotheses, we used least squares linear three-way ANOVA models to test the individual and interactive effects of station, depth, and season on concentrations of nutrients, Chl *a* and bacterioplankton to evaluate differential enrichment or depletion of parameters along depth profiles. We additionally performed post hoc tests (Tukey HSD) to examine all pairwise comparisons for depth, station, and the interaction of depth and station. Visualizations of the data and all statistics were carried out in MATLAB (Release 2022a, The MathWorks, Inc.).

Results

Climatological data: *Kau* and *Ho'oilo*

Wind speed varied significantly between the two seasons ($p < 0.0005$), but there was no significant seasonal difference in daily rainfall ($p = 0.6051$) (Supporting Information Fig. S2). The mean wind speed during *kau* was 4.60 m s^{-1} (SD 1.40) and the mean wind speed during *ho'oilo* was 4.07 m s^{-1} (SD 1.67). During *kau*, trade winds (from 10° to 90°) occurred during 80.8% of days. During *ho'oilo*, trade winds occurred on only 58.5% of days.

Spatial trends in physical and biogeochemical parameters

Linear models revealed significant trends in nitrate + nitrite, phosphate, and Chl *a* concentrations with depth and distance from shore at alpha = 0.05 (Supporting Information Table S1). Nitrate + nitrite was very low in the mixed layer at all sites and increased with depth, as is typical for oligotrophic systems (Fig. 2a; Supporting Information Fig. S3). At 75 and 100 m sampling depths, there was significant enhancement of nitrate at S1 and S2 compared to S3 (Fig. 2a; Supporting Information Fig. S3; Supporting Information Table S2). Phosphate was also low in the mixed layer, and S1 was elevated in phosphate compared to S3 at 75, 100, and 125 m (Fig. 2b; Supporting Information Table S2). At 100 m, phosphate at S2 was significantly higher than at S3 (Fig. 2b; Supporting Information Table S2). Silicate was present in the mixed layer at all three sites (Fig. 2c). The silicate profile was similar between the three stations except at 75 m, it was significantly enhanced at S1 compared to S3 at = 0.005 (Fig. 2c; Supporting Information Table S2).

Chl *a* concentrations were highest at the nearshore S1, decreased at S2, and were lowest at oceanic Sta. S3, as expected for a tropical island with an island mass effect. S1 was significantly enhanced in Chl *a* compared to S3 at depths of 5–75 m, and was significantly enhanced compared to the 6.5 km station at 25–75 m (Fig. 2d; Supporting Information Table S2). S2 was significantly enhanced in Chl *a* compared to S3 at depths of 5–100 m (Fig. 2d; Supporting Information Table S2). Chl *a* data from surface bottle samples and VIIRS satellite data showed similar trends in station and seasonality (Supporting Information Fig. S4).

The depth of the DCM increased with distance from shore. The mean depth of the DCM at S1 was shallower than both S2 and S3 (Fig. 3; Table 1; Supporting Information Table S3). The DCM at S2 was also significantly shallower than at S3 (Supporting Information Table S3). The mean depth of the DCM trended slightly shallower during *ho'oilo* than during *kau* at all stations by a mean of about 7–8 m, but the statistical significance was marginal (Supporting Information Table S3).

Typically the MLD was slightly deeper at S3 compared to the nearshore stations, and this difference was significant between S3 and the S1 (Table 1; Supporting Information Table S3). The MLD was consistently shallower than the DCM and was on average deeper in *ho'oilo* than in *kau* (Supporting Information Table S3). Similar to the mixed layer depth, the depth where photosynthetically active radiation was 1% and 0.1% of surface levels also increased with distance from shore (Table 1; Supporting Information Table S3).

The average buoyancy frequency in three regions (surface, within DCM, and below DCM) was calculated for each cast with a clear DCM feature, which included 50% of casts at S1, 50% of casts at the 6.5 km station, and 100% of casts at the 100 km station (Sta. ALOHA). The mean buoyancy frequency in the DCM layer was higher than the buoyancy frequency above and below the DCM layer ($p < 0.001$ and $p = 0.049$, respectively), and the lowest buoyancy frequencies were observed at the surface layer ($p < 0.001$) (Table 2; Supporting Information Table S3). The DCM was typically found in or just below the region of highest buoyancy frequency, which indicates a region with a stronger pycnocline (Fig. 3). The buoyancy frequency was less variable at S3 than at S1 and S2, especially in the DCM and below (Table 2).

Onshore–offshore gradients in picoplankton

Linear models relating cell count to depth, station, and the interaction of depth and station revealed significant effects for each cell type at alpha = 0.05, with the exception of the depth: station interaction for heterotrophic bacteria (Supporting Information Table S4). Post-hoc Tukey's HSD test results are reported in the following paragraphs and Supporting Information Table S5.

Prochlorococcus mean cell concentrations increased with distance from shore at all depths. Compared to S3, *Prochlorococcus* was significantly enriched at S1 at 75–125 m (Fig. 4a; Supporting Information Table S5). At all stations, the *Prochlorococcus* population began to significantly decrease between 75 and 100 m (Fig. 4a). In the surface layer, *Prochlorococcus* concentrations at S1 and S2 were 77% and

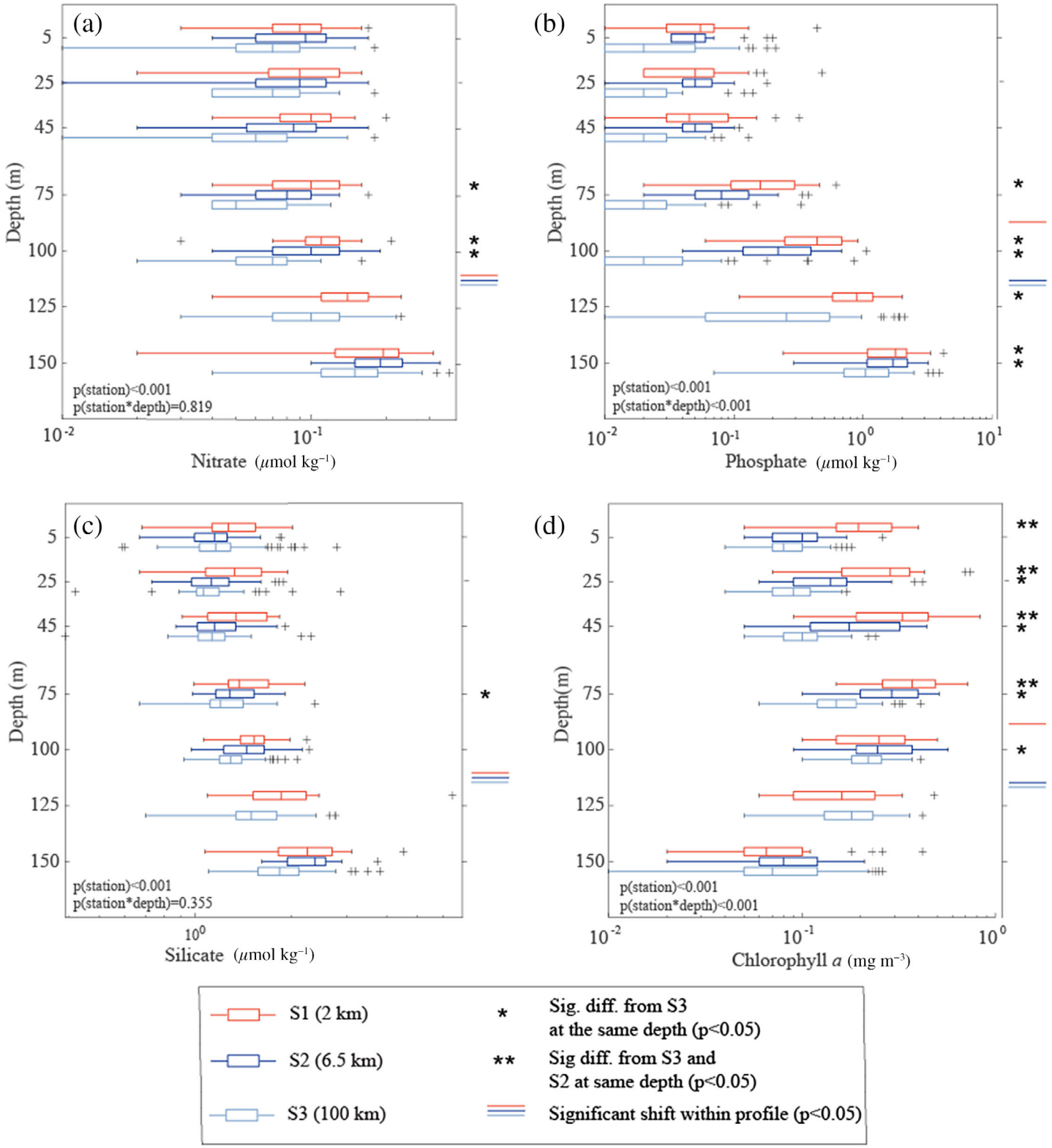

Fig. 2. Profiles at each site for (**a**) nitrate + nitrite, (**b**) phosphate, (**c**) silicate, and (**d**) chlorophyll *a*. Error bars represent ± 1 standard deviation. Red represents S1, dark blue represents S2, and light blue represents S3.

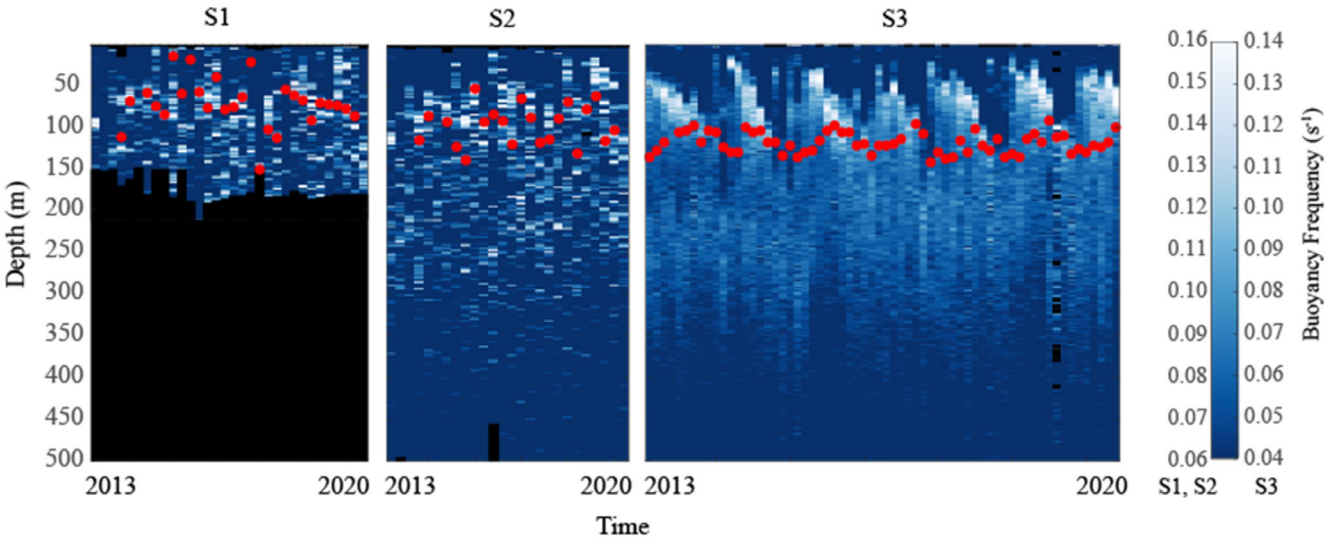

Fig. 3. Buoyancy frequency profiles and chlorophyll maximum for each cast at three stations. The red dot indicates the maximum chlorophyll observation in the profile. Lighter colors indicate higher buoyancy frequency, meaning areas of relatively rapid change in density. Black indicates areas with no data, either due to depth limitation at S1, or missing density data. Each column represents a single cast in order of time.

90% of that at S3, respectively. Near the DCM (~ 75 m), the mean *Prochlorococcus* concentration at S1 was 50% of the mean concentration at S3, and at S2 it was 70% of the concentration at S3.

Synechococcus concentrations decreased from nearshore to oceanic waters, opposite of the trend observed for *Prochlorococcus*, though overall *Prochlorococcus* was more abundant than *Synechococcus* at all depths and all stations (Fig. 4b; Supporting Information Table S5). *Synechococcus* nearshore enhancement was highest at the surface, with mean concentrations 8.5 times and 3.6 times higher than S3 at S1 and S2, respectively. Significant enhancement of *Synechococcus* was noted at S1 relative to S3 within the upper mixed layer (depths from 5 to 45 m; Fig. 4b; Supporting Information Table S5). *Synechococcus* population densities were also much more variable in the nearshore environment than in the open ocean (Fig. 4b). The ratio of *Prochlorococcus* : *Synechococcus* cell abundances increased with distance from shore (Supporting Information Fig. S5).

Picoeukaryotes followed a similar trend to *Synechococcus*, with an increase in population moving from nearshore to oceanic waters (Fig. 4c; Supporting Information Table S5). Picoeukaryote enhancement in nearshore waters was significant from 5 to 75 m at both S1 and S2. S2 and S3 both had significant subsurface maxima in picoeukaryotes, with the 6.5 km maxima occurring at 75–100 m and the 100 km maxima occurring at 100–125 m.

Heterotrophic bacteria abundances did not show a trend in mean cell abundance from onshore to offshore. At all three stations, heterotrophic bacteria populations significantly

Table 1. Means and standard deviations of the depth of the deep chlorophyll maximum (DCM), mixed layer depth (MLD), depth of 1% light, and depth of 0.1% light during *kau* (May–October) and *ho'oilo* (November–April) at three stations, from profiles taken quarterly (2 km, 6 km locations) and monthly (Sta. ALOHA) between 2013 and 2020. The mean depth of the DCM and both light levels differed significantly among all three stations but did not differ between seasons. The mixed layer depth differed significantly between S1 and S3 and between seasons. Results of statistical comparisons of the means are in Supporting Information Table S3.

Parameter	Season	Depth (m) at S1	Depth (m) at S2	Depth (m) at S3
DCM	*Kau*	74.9 ± 24.9	99.1 ± 27.0	122.7 ± 10.5
	Ho'oilo	67.1 ± 35.0	91.0 ± 15.0	114.3 ± 13.3
MLD	*Kau*	37.2 ± 14.6	42.7 ± 19.2	43.9 ± 13.7
	Ho'oilo	52.1 ± 37.2	49.6 ± 22.5	69.8 ± 26.5
1% Light	*Kau*	84 ± 16	93 ± 18	103 ± 9
	Ho'oilo	75 ± 14	86 ± 20	103 ± 9
0.1% Light	*Kau*	127 ± 21	142 ± 19	154 ± 10
	Ho'oilo	120 ± 19	133 ± 24	154 ± 12

Table 2. Means and standard deviation of buoyancy frequency for the three depth bins, and depth and thickness of DCM at each station.

	Buoyancy frequency (± SD) (s^{-1})				
	Top 20 m	DCM layer	Below DCM	Depth of DCM (m)	Thickness of DCM (m)
S1	0.032 ± 0.025	0.068 ± 0.047	0.045 ± 0.033	75.6 ± 15.7	68.3 ± 14.1
S2	0.017 ± 0.021	0.072 ± 0.044	0.049 ± 0.032	92.3 ± 25.1	58.9 ± 21.3
S3	0.019 ± 0.017	0.064 ± 0.013	0.056 ± 0.007	118.6 ± 12.5	67.1 ± 24.5

decreased below 75 m. There was higher variability at all depths at the 2 km station compared to the 6 and 100 km stations (Fig. 4d).

Plots of cell counts over time at S1 and S3 are shown in Fig. 5 (S2 is omitted because of data gaps due to sea conditions). Sampling at the nearshore sites was quarterly, and sampling at S3 was approximately monthly. The high temporal variability in *Prochlorococcus* at S3 (Fig. 5e) suggests that nearshore variability in *Prochlorococcus* could be missed at the quarterly sampling interval. At both stations, the maximum *Prochlorococcus* concentrations are found above the DCM (Fig. 5a,e). *Synechococcus* was generally low at S3, but at S1 there are sporadic high concentrations in the surface waters (Fig. 5b,f). Elevated *Synechococcus* concentrations, like *Prochlorococcus*, occur shallower than the DCM at both stations (Fig. 5b,f).

Picoeukaryotes were higher at S1 than S3 throughout the sampling period, but at both stations, the maximum abundance of picoeukaryotes often occurred within or near the DCM depth (Fig. 5c,g), in contrast to *Synechococcus* and *Prochlorococcus* which consistently had maxima shallower than the DCM. Finally, while the mean heterotrophic bacteria concentrations were similar at nearshore and offshore sites (Fig. 4d), there was higher variability in the nearshore site driven by occasional population spikes at 25, 45, or 75 m. This variability was less pronounced at S3 (Fig. 5d,h).

The patterns in buoyancy frequency changed from nearshore to offshore (Fig. 3). S1 and S2 consistently had multiple locations of rapidly changing density and buoyancy frequency, and S3 typically had higher buoyancy frequencies clustered together in a clear pycnocline. This indicates a less stable water column in the near-island environment compared to S3. Higher *Synechococcus* and picoeukaryote concentrations were found in the less stably stratified water of S1 and S2, and the opposite was found for *Prochlorococcus*, with higher populations observed in the more stably stratified water of S3.

Seasonality of picoplankton concentrations, nutrients, and chlorophyll

Statistical models that included station, depth, season, and all interaction terms revealed several seasonal trends (Supporting Information Tables S1, S4). Overall, Chl *a* observations were higher in *ho'oilo* than *kau* ($p < 0.001$, $f = 51.365$), and the interaction of season and station was also significant ($p = 0.003$, $f = 5.86$). There was a significant seasonal effect in heterotrophic bacteria populations with *ho'oilo* numbers lower than *kau* numbers when averaging over all depths and stations ($p < 0.001$, $f = 45.017$). Few significant seasonal trends were observed for nutrients, picoeukaryotes, *Synechococcus*, and *Prochlorococcus*. At S3 during *ho'oilo*, there was significantly higher phosphate at 150 m ($p = 0.020$) and higher *Synechococcus* at 125 m ($p = 0.048$).

Shifts in contribution to total carbon among picoplankton types

The estimated carbon contribution of all picoplankton types was calculated to determine the relative contribution of each cell type to overall picoplankton biomass. S1 had a lower carbon contribution from *Prochlorococcus* and higher contribution from *Synechococcus* and picoeukaryotes compared to S2 and S3 (Fig. 6d–f). As expected, below the DCM, the relative contribution of heterotrophic bacteria to the picoplankton biomass becomes greater (Fig. 6). By calculating the total integrated biomass throughout the water column from 0 to 150 m, we see a slightly higher estimated biomass at S3 compared to the nearshore stations (S1: 1351 ± 308 mg C m^{-2}; S2 1330 ± 231 mg C m^{-2}; S3: 1481 ± 181 mg C m^{-2}). In terms of picophytoplankton biomass, the higher abundance of *Prochlorococcus* compensated for the lower concentrations of *Synechococcus* and picoeukaryotes S3 compared to S1 and S2, and the 0–150 m integrated water column carbon estimates for the picophytoplankton increase slightly moving offshore (S1: 666 ± 174 mg C m^{-2}; S2: 717 ± 200 mg C m^{-2}; S3: 742 ± 112 mg C m^{-2}).

Discussion

In this study, the IME was observed at O'ahu, Hawai'i via significant Chl *a* enhancement at near-island S1 and S2 relative to the oceanic S3 (Fig. 2d). As a high volcanic island in the trade wind latitudes and the most heavily populated island in Hawai'i, O'ahu experiences both physical and anthropogenic forcings likely to contribute to the IME. Nutrients that allow phytoplankton growth were observed in higher concentrations at 75–100 m near O'ahu compared to S3 (Fig. 2a,b). These nutrients could be introduced to the mixed layer near O'ahu by island-generated internal waves

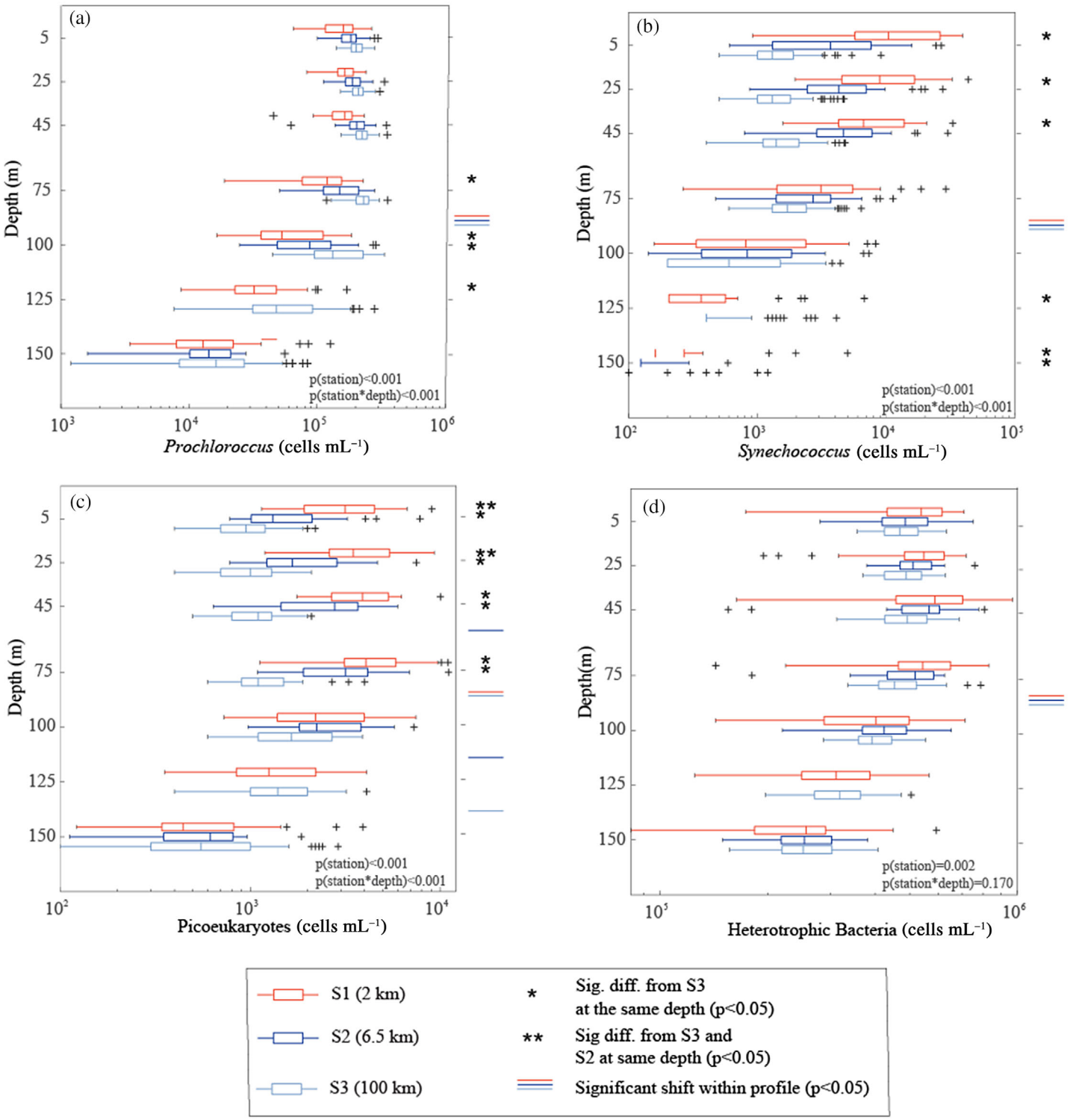

Fig. 4. Concentrations of (**a**) *Prochlorococcus* (cells mL^{-1}) vs. depth (m); (**b**) *Synechococcus* (cells mL^{-1}) vs. depth; (**c**) picoeukaryotes (cells mL^{-1}) vs. depth and (**d**) heterotrophic bacteria (cells mL^{-1}) vs. depth. S1 is shown in red, S2 in dark blue, and S3 in light blue. Box plots show the 25th, 50th, and 75th percentile and outliers are indicated with plus signs.

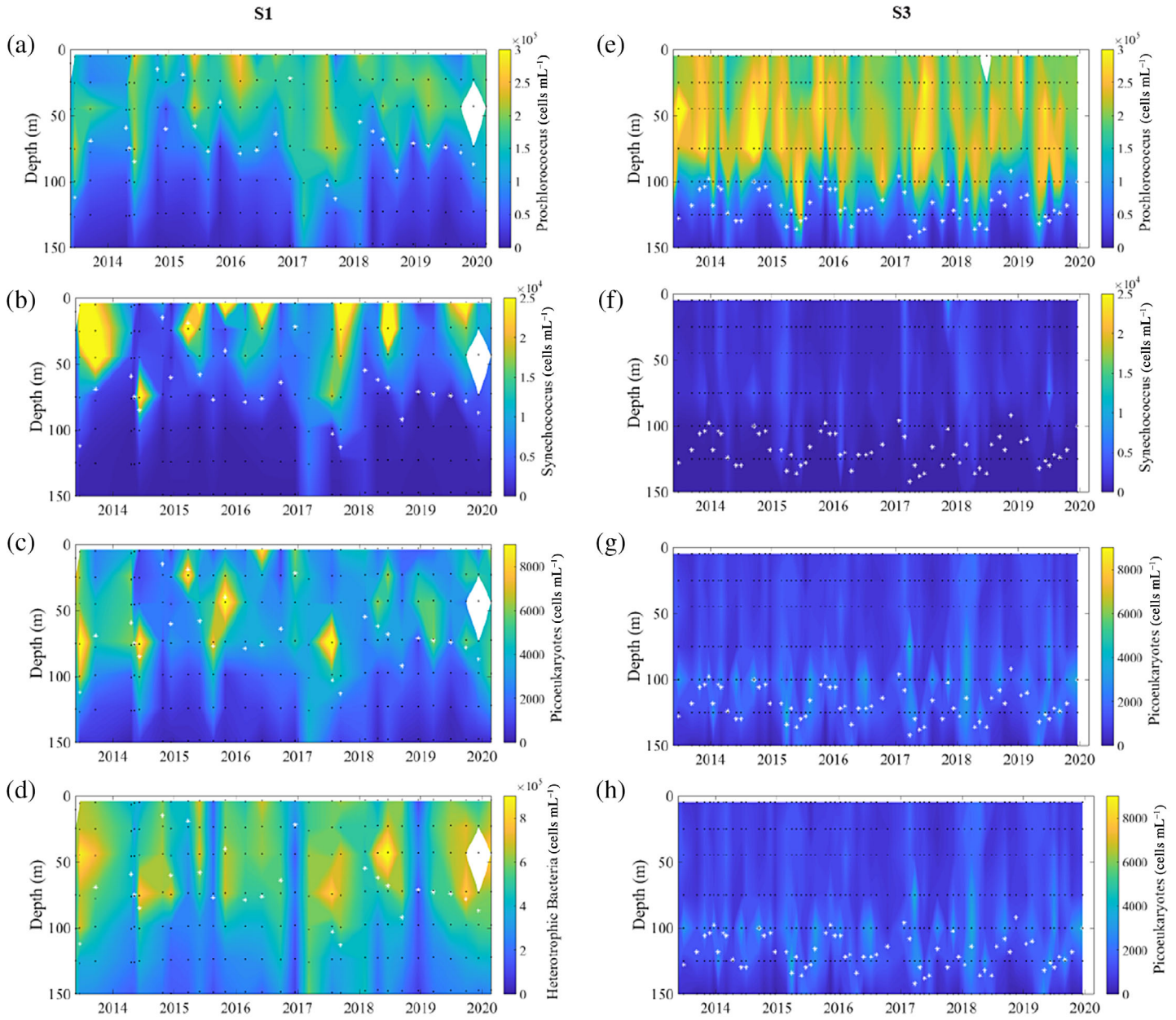

Fig. 5. Profiles of picoplankton concentration (cells mL^{-1}) shown by time (yr) vs. depth (m). The left column shows data from S1 for (**a**) *Prochlorococcus*, (**b**) *Synechococcus*, (**c**) picoeukaryotes, and (**d**) heterotrophic bacteria. The right column shows data from S3 for (**e**) *Prochlorococcus*, (**f**) *Synechococcus*, (**g**) picoeukaryotes, and (**h**) heterotrophic bacteria. Each sample is represented by a black dot. The deep chlorophyll maximum for each cast is located by a white star. The cell concentrations are on the color axis, with yellow as high relative abundance and blue as low relative abundance. Note that for each picoplankton type, the color axis range is different.

combined with wind-driven deep mixing or terrigenous riverine or groundwater solute fluxes including nonpoint source pollution from farming and development or point source pollution from wastewater treatment plant outfalls (Gove et al. 2016).

Around O'ahu, internal waves are generated at the flanks of ridges at the southeastern corner and north of the island (Eich et al. 2004) and these internal waves propagate around the island and cause shoaling of isopycnals at tidal frequencies within Māmala Bay (Comfort et al. 2015). Isopycnal shoaling has been observed to bring waters with nitrate concentrations of 8–16 μmol kg^{-1} into the photic zone on the south shore of O'ahu (Comfort et al. 2015). Also, high-amplitude internal waves propagating through the open ocean can break when they interact with island slopes, causing turbulence and mixing, which can introduce nutrients to the mixed layer

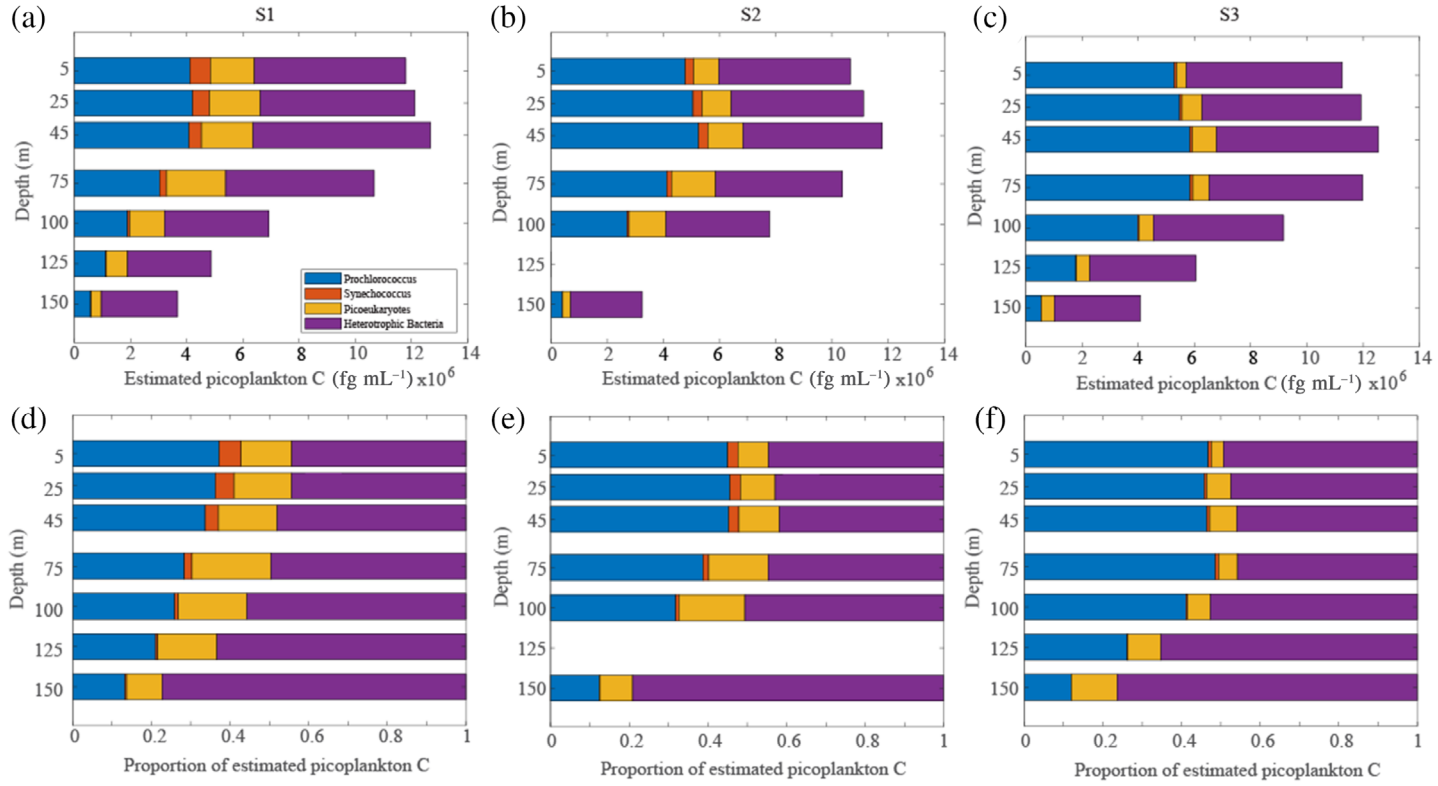

Fig. 6. Estimates of carbon content contributed by each picoplankton type (*Prochlorococcus*, *Synechococcus*, picoeukaryotes, and heterotrophic bacteria, designated by color). The carbon estimates are shown as total picoplankton carbon (**a–c**) and proportion of total picoplankton carbon (**d–f**). Estimates are shown for each long-term monitoring station: S1 (**a**, **d**), S2 (**b**, **e**), and S3 (**c**, **f**).

and euphotic zone (Wolanski and Delesalle 1995; Leichter and Genovese 2006; Reid et al. 2019), especially when combined with wind-driven mixing (van den Engh et al. 2017). Buoyancy frequency was more variable at the nearshore stations than at S3, indicating lower water column stability and the potential for more mixing of nutrients into the euphotic zone at S1 and S2 compared to the more consistently stratified waters of S3 (Fig. 3). The DCM was located either at the top of or within the pycnocline, indicating the presence of more nutrients in that region of the water profile.

We also observed a significant increase in Chl *a* in the near-surface waters, especially at S1 only 2 km from shore (Fig. 2d). Land-based nutrient inputs may also play a significant role in generating the IME on O'ahu. In addition to natural lithology dissolution, O'ahu has many point and non-point sources of nutrients that originate on land, including stormwater and wastewater discharge.

On O'ahu, regular heavy rainfall events cause increased stream flow and stormwater runoff with high nutrient concentrations from fertilizers and animal waste (Hoover and Mackenzie 2009). Non-point source wastewater pollution is a significant contributor to nutrient enrichment in O'ahu's groundwater, since the island has over 11,000 cesspools that leach ~ 7.5 million gallons d^{-1} of untreated wastewater (The State of Hawai'i Department of Health-Environmental Management Division, 2017) along with aging and corroded sewer infrastructure. Although stormwater and non-point source nutrient pollution can become trapped in estuaries, a study of nutrients in Māmala Bay found that nitrate + nitrite concentrations up to 2 μmol kg^{-1} were found outside the mouths of Pearl Harbor and the Ala Wai canal, indicating transport of nutrients out of the estuaries (Laws et al. 1999). Also, many studies have observed horizontal advection of reef water to island slopes and oceanic waters via wind/wave forcing and tidal flushing of backreef areas and lagoons (Aucan et al. 2021; Vollbrecht et al. 2021; Comstock et al. 2022), so coastal waters are enriched with terrigenous nutrients.

Nearshore Chl *a* and phytoplankton concentrations may also be influenced by point source nutrient pollution impacts to Māmala Bay from two municipal wastewater treatment plants, which together discharge about 97 million gallons d^{-1} of nutrient-rich treated wastewater to the bay at depths of about 60–70 m (City and County of Honolulu, Department of Environmental Services). The wastewater plumes have nitrate + nitrite concentrations of 5.7 ± 8.1 and 7.7 ± 2.8 μmol L^{-1} and phosphate concentrations of 72 ± 3 and 54 ± 8 μmol L^{-1} (Laws et al. 1999). This nutrient input has been found to influence local concentrations of Chl *a*,

Synechococcus, and heterotrophic bacteria (Vedernikov et al. 2007) and increase phytoplankton growth rates (Petrenko 1997).

Picoplankton community structure, IME, and water column stability

Photoautotroph distribution and abundance is influenced by water column stability (Schmoker and Hernandez-Leon, 2013; Silovic et al., 2018) in addition to temperature (Mackey et al. 2013) and biogeochemistry (Moore et al., 2002). Previous studies have shown that picophotoautotrophs thrive in more stratified system and larger photoautotrophs dominate in less stratified systems (Schomker and Hernandez-Leon, 2013), and additionally within the picophytoplankton there is niche partitioning based on physical and chemical properties of the water column (Silovic et al. 2018, Sohm et al. 2016). In this study, we observed that *Prochlorococcus* concentrations decreased moving closer to shore while *Synechococcus* and picoeukaryote concentrations increased (Fig. 4). These observations were most pronounced in the deeper photic zone (75–125 m) for *Prochlorococcus* and in the mixed layer and shallower photic zone for *Synechoccus* and picoeukaryotes. This means that the increase in concentrations of *Synechococcus* and picoeukaryotes moving toward shore tracked a similar increase in Chl *a*, an increase in nitrate + nitrite and phosphate (Fig. 2a,b) and decrease in water column stability (Fig. 3). The higher concentrations of nutrients toward the base of the depth range of *Synechococcus* and picoeukaryotes, combined with elevated cell counts throughout the upper water column suggest that nutrients are being introduced to the euphotic zone at S1 and S2 and are utilized by *Synechococcus* and picoeukaryotes. Evidence of these elevated nutrient concentrations is visible at 75–100 m (Fig. 2a,b) where *Synechococcus* and picoeukaryotes begin to experience light limitation.

Prochlorococcus concentrations, conversely, had a negative relationship with Chl *a*, nitrate + nitrite, and phosphate, and a positive relationship with water column stability. Since most *Prochlorococcus* strains are unable to use nitrate as a source of N, instead relying primarily on ammonium and other remineralized forms of N (Moore et al. 2002; Berube et al. 2023), they are unable to utilize the nitrate that is introduced to the euphotic zone near the island, unlike *Synechococcus* and picoeukaryotes. Also, it has been suggested that *Prochlorococcus* is better suited for highly stratified, stable water columns whereas *Synechococcus* can thrive in less stable water columns (Bird and Wyman 2003), and our observations of cell counts and buoyancy frequency align with this hypothesis.

While most previous observations of the IME in oligotrophic ocean basins have focused on satellite and shipboard observations of Chl *a* enhancement surrounding islands (Caldeira et al. 2002; Andrade et al., 2014; Gove et al. 2016; Vollbrecht et al. 2021) and shipboard sampling of larger phytoplankton (Gilmartin and Revelante 1974; Shiozaki et al. 2014), some recent studies have also investigated picoplankton spatial trends near islands. A recent study in Kane'ohe Bay, a large and well-studied embayment on O'ahu's eastern coast, also examined picoplankton spatial distributions and found similar trends to this study (Tucker et al. 2021). *Prochlorococcus* concentrations in the coastal zone (1–2 km from shore) were extremely low; at sites located 4–7 km from shore, the cell numbers increased. *Synechococcus*, picoeukaryotes, and Chl *a* were highest at the coastal sites and decreased moving away from the island. In contrast to the present study, they observed a gradient in heterotrophic bacteria with highest numbers at the coastal sites (Tucker et al. 2021). Similar trends in *Prochlorococcus* and *Synechococcus* trends from reef to offshore were observed in Mo'orea and Tahiti in French Polynesia (Comstock et al. 2022), indicating that this shift in the bacterioplankton community composition due to the IME may be found widely throughout the ocean basins.

Seasonality

Seasonality in the picoplankton community has previously been examined at S3 (Sta. ALOHA). In a study taking place during the 1991–1994 ENSO, *Synechococcus* maxima occurred in winter, picoeukaryotes occurred in spring, and *Prochlorococcus* in the summer to fall (Campbell et al. 1997). Malmstrom et al. (2010) found similar patterns in seasonal abundances in 2003–2008. In the current study, we chose to use the traditional Hawaiian seasonal distinctions of *kau* and *ho'oilo*, which roughly correspond to winter and summer, and we also found that *Synechococcus* was higher in the winter at S3, though this was not observed at the nearshore stations.

We propose potential reasons for the stronger seasonal patterns in *Synechococcus* at S3: (1) land-based nutrient input and weaker stratification that may lead to increased *Synechococcus* populations nearshore compared to the open oligotrophic ocean and are likely to occur year-round; (2) stronger trade winds (Fig. 2) and higher surf from Antarctic storms are observed in Māmala Bay in the summer and may allow more frequent entrainment of deep-water nutrients into the photic zone, which could cause summer pulses of phytoplankton; and (3) Māmala Bay is protected from the north Pacific winter storms that generate deep mixing events at S3 (van den Engh et al. 2017) because of shielding from the island.

Carbon fixation, trends in integrated biomass, and relationship to increased chlorophyll observations near islands

We observed that the biomass of picoplankton did not increase close to the island, but larger picophytoplankton (*Synechococcus* and picoeukaryotes) were significantly enhanced while the smallest phytoplankter *Prochlorococcus* was depleted. We also observed enhanced Chl *a* at S1 compared to S2, and both near-island sites had enhanced Chl *a* compared to the open-ocean S3. Chl *a* increases near islands

are generally associated with increased biomass (e.g., Gove et al. 2016). Since we did not observe an increase in biomass in the picoplankton population but did observe that larger phytoplankton were relatively more abundant in the nearshore environment compared to the offshore environment, the observed increases in Chl *a* (observed in both water samples and satellite data) are likely driven by larger phytoplankton groups such as diatoms and dinoflagellates. Shipboard plankton surveys near islands have long observed higher productivity and different community partitioning of larger plankton compared to offshore and oceanic stations. These trends have been observed throughout the global ocean including near Hawai'i (Gilmartin and Revelante 1974), the Barbados islands (Sander and Steven 1973), the Prince Edward Archipelago (Boden 1988), and the western subtropical Pacific (Shiozaki et al. 2014).

The broader implications of the increased primary production near islands due to the IME range from understanding localized nearshore pollution impacts (D'Costa et al. 2017) to global carbon budgets (Field et al. 1998). Natural processes can introduce nutrients from islands to the nearshore ecosystem, but in Hawai'i, development, agriculture, invasive ungulates and other mammals all work together to create an excessive nutrient load to the nearshore environment (Foo et al. 2021; Gove et al. 2023). This can be devastating to Hawai'i's coral reef ecosystems, but the additional nutrient input may also alter phytoplankton community structure and water characteristics. In the Pacific region, climate change has the potential to disrupt key ecological processes that affect the nearshore and oceanic marine environment. Changes in the frequency and intensity of trade winds (Xiang et al. 2014; Li et al. 2019) would change the number of deep mixing events and alter water column stability. This could alter the proportion of the observed IME that is driven by oceanographic processes and additionally influence picophytoplankton dynamics. With increasing land-based pollution driven by development and sea-level rise combined with changes in the frequency and intensity of deep mixing events, further research could help predict the trajectory of nearshore biomass enhancement near the Hawai'i by determining how much biomass enrichment is due to land-based vs. oceanographic forcing. In addition, near-island fisheries are constrained by the amount of primary production that occurs near island, so future shifts in the amount of biomass enhancement could have cascading impacts throughout the food web, including subsistence fisheries and local food security (Hays et al. 2005).

Conclusions

This study quantifies shifts in picoplankton community structure between nearshore waters of O'ahu and oceanic waters near Hawai'i. We investigated the location of the deep chlorophyll maximum relative to the buoyancy frequency profile instead of the mixed layer depth and found that the DCM is typically located in regions with higher buoyancy frequency (pycnocline), highlighting that the physical structure of the water column, in addition to light and nutrient availability, is an important factor in determining the location of DCM features. We found a shift in the picoplankton ratios, with higher concentrations of *Synechococcus* and picoeukaryotes close to shore but lower concentrations of *Prochlorococcus*, compared to the oceanic site at Sta. ALOHA. Seasonality was observed, particularly for *Synechococcus* with winter enhancement in oceanic waters. Despite the enhancement in the *Synechococcus* and picoeukaryote populations near shore, the estimated carbon biomass in the picoplankton community as a whole did not show any enhancement at the nearshore sites. We did observe enhanced Chl *a* near the island, so this suggests that the productivity enhancements observed near shore are likely due to increased numbers of larger phytoplankton classes that were not enumerated here. This study contributes to the growing understanding of the dynamics and persistence of the IME in Hawai'i, with implications for better understanding island pollution management, global carbon budgets, and fisheries production near island ecosystems.

Data availability statement

All data referenced in this study are available online at the website of the Laboratory for Microbial Oceanography at the University of Hawai'i at Mānoa. Nearshore data can be found here: https://hahana.soest.hawaii.edu/cmoreswac/cmoreswac.html. Sta. ALOHA data can be found here: https://hahana.soest.hawaii.edu/hot/hot-dogs/interface.html.

References

Andrade, I., P. Sangrà, S. Hormazabal, and M. Correa-Ramirez. 2014. Island mass effect in the Juan Fernández Archipelago (33°S), Southeastern Pacific. Deep-Sea Res. I: Oceanogr. Res. Pap. **84**: 86–99. doi:10.1016/j.dsr.2013.10.009

Arístegui, J., P. Sangrá, S. Hernández-León, M. Cantón, A. Hernández-Guerra, and J. L. Kerling. 1994. Island-induced eddies in the Canary islands. Deep-Sea Res. I: Oceanogr. Res. Pap. **41**: 1509–1525. doi:10.1016/0967-0637(94)90058-2

Armstrong, F. A. J., C. R. Stearns, and J. D. H. Strickland. 1967. The measurement of upwelling and subsequent biological process by means of the Technicon Autoanalyzer® and associated equipment. Deep-Sea Res. Oceanogr. Abstr. **14**: 381–389. doi:10.1016/0011-7471(67)90082-4

Aucan, J., T. Desclaux, R. Le Gendre, V. Liao, and S. Andréfouët. 2021. Tide and wave driven flow across the rim reef of the atoll of Raroia (Tuamotu, French Polynesia). Mar. Pollut. Bull. **171**: 112718. doi:10.1016/j.marpolbul.2021.112718

Berube, P. M., T. J. O'Keefe, A. Rasmussen, T. LeMaster, and S. W. Chisholm. 2023. Production and cross-feeding of nitrite within *Prochlorococcus* populations. mBio **14**: e0123623. doi:10.1128/mbio.01236-23

Biller, S. J., P. M. Berube, D. Lindell, and S. W. Chisholm. 2015. *Prochlorococcus*: The structure and function of collective diversity. Nat. Rev. Microbiol. **13**: 13–27. doi:10.1038/nrmicro3378

Bird, C., and M. Wyman. 2003. Nitrate/nitrite assimilation system of the marine picoplanktonic cyanobacterium *Synechococcus sp*. strain WH 8103: Effect of nitrogen source and availability on gene expression. Appl. Environ. Microbiol. **69**: 7009–7018. doi:10.1128/AEM.69.12.7009-7018.2003

Boden, B. P. 1988. Observations of the island mass effect in the Prince Edward archipelago. Polar Biol. **9**: 61–68. doi:10.1007/BF00441765

Caldeira, R. M. A., S. Groom, P. Miller, D. Pilgrim, and N. P. Nezlin. 2002. Sea-surface signatures of the island mass effect phenomena around Madeira Island, Northeast Atlantic. Remote Sens. Environ. **80**: 336–360. doi:10.1016/S0034-4257(01)00316-9

Campbell, L., and D. Vaulot. 1993. Photosynthetic picoplankton community structure in the subtropical North Pacific Ocean near Hawaii (station ALOHA). Deep-Sea Res. I: Oceanogr. Res. Pap. **40**: 2043–2060. doi:10.1016/0967-0637(93)90044-4

Campbell, L., H. Liu, H. A. Nolla, and D. Vaulot. 1997. Annual variability of phytoplankton and bacteria in the subtropical North Pacific Ocean at station ALOHA during the 1991–1994 ENSO event. Deep-Sea Res. I: Oceanogr. Res. Pap. **44**: 167–192. doi:10.1016/S0967-0637(96)00102-1

Casey, J. R., K. M. Björkman, S. Ferrón, and D. M. Karl. 2019. Size dependence of metabolism within marine picoplankton populations. Limnol. Oceanogr. **64**: 1819–1827. doi:10.1002/lno.11153

Chavez, F. P., K. R. Buck, R. R. Bidigare, D. M. Karl, D. Hebel, M. Latasa, L. Campbell, and J. Newton. 1995. On the chlorophyll *a* retention properties of glass-fiber GF/F filters. Limnol. Oceanogr. **40**: 428–433. doi:10.4319/lo.1995.40.2.0428

Chisholm, S. W., S. L. Frankel, R. Goericke, R. J. Olson, B. Palenik, J. B. Waterbury, L. West-Johnsrud, and E. R. Zettler. 1992. *Prochlorococcus marinus* nov. gen. nov. sp.: An oxyphototrophic marine prokaryote containing divinyl chlorophyll *a* and *b*. Arch. Microbiol. **157**: 297–300. doi:10.1007/BF00245165

Comfort, C. M., M. A. McManus, S. J. Clark, D. M. Karl, and C. E. Ostrander. 2015. Environmental properties of coastal waters in Mamala Bay, Oahu, Hawaii, at the future site of a seawater air conditioning outfall. Oceanography **28**: 230–239. doi:10.5670/oceanog.2015.46

Comstock, J., C. E. Nelson, A. James, E. Wear, N. Baetge, K. Remple, A. Juknavorian, and C. A. Carlson. 2022. Bacterioplankton communities reveal horizontal and vertical influence of an island mass effect. Environ. Microbiol. **24**: 4193–4208. doi:10.1111/1462-2920.16092

Dandonneau, Y., and L. Charpy. 1985. An empirical approach to the island mass effect in the south tropical Pacific based on sea surface chlorophyll concentrations. Deep-Sea Res. A: Oceanogr. Res. Pap. **32**: 707–721. doi:10.1016/0198-0149(85)90074-3

D'Costa, P. M., M. S. D'Silva, and R. K. Naik. 2017. Impact of pollution on phytoplankton and implications for marine econiches, p. 205–222. *In* M. M. Naik and S. K. Dubey [eds.], Marine pollution and microbial remediation. Springer. doi:10.1007/978-981-10-1044-6_13

De Falco, C., F. Desbiolles, A. Bracco, and C. Pasquero. 2022. Island mass effect: A review of oceanic physical processes. Front. Mar. Sci. **9**: 894860. doi:10.3389/fmars.2022.894860

Doty, M. S., and M. Oguri. 1956. The island mass effect. ICES J. Mar. Sci. **22**: 33–37. doi:10.1093/icesjms/22.1.33

Eich, M. L., M. A. Merrifield, and M. H. Alford. 2004. Structure and variability of semidiurnal internal tides in Mamala Bay, Hawaii. J. Geophys. Res.: Oceans **109**. doi:10.1029/2003jc002049

Field, C. B., M. J. Behrenfeld, J. T. Randerson, and P. Falkowski. 1998. Primary production of the biosphere: Integrating terrestrial and oceanic components. Science **281**: 237–240. doi:10.1126/science.281.5374.237

Foo, S. A., W. J. Walsh, J. Lecky, S. Marcoux, and G. P. Asner. 2021. Impacts of pollution, fishing pressure, and reef rugosity on resource fish biomass in West Hawaii. Ecol. Appl. **31**: e2213. doi:10.1002/eap.2213

Gilmartin, M., and N. Revelante. 1974. The 'island mass' effect on the phytoplankton and primary production of the Hawaiian Islands. J. Exp. Mar. Biol. Ecol. **16**: 181–204. doi:10.1016/0022-0981(74)90019-7

Gove, J. M., and others. 2016. Near-island biological hotspots in barren ocean basins. Nat. Commun. **7**: 10581. doi:10.1038/ncomms10581

Gove, J. M., and others. 2023. Coral reefs benefit from reduced land–sea impacts under ocean warming. Nature **621**: 536–542. doi:10.1038/s41586-023-06394-w

Grasshoff, K., M. Ehrhardt, and K. Kremling [eds.]. 1983. Methods of seawater analysis. Verlag Chemie.

Hays, G. C., A. J. Richardson, and C. Robinson. 2005. Climate change and marine plankton. Trends Ecol. Evol. **20**: 337–344. doi:10.1016/j.tree.2005.03.004

Hench, J. L., J. J. Leichter, and S. G. Monismith. 2008. Episodic circulation and exchange in a wave-driven coral reef and lagoon system. Limnol. Oceanogr. **53**: 2681–2694. doi:10.4319/lo.2008.53.6.2681

Hernández-León, S. 1991. Accumulation of mesozooplankton in a wake area as a causative mechanism of the "island-mass effect". Mar. Biol. **109**: 141–147. doi:10.1007/BF01320241

Hoover, D. J., and F. T. Mackenzie. 2009. Fluvial fluxes of water, suspended particulate matter, and nutrients and potential impacts on tropical coastal water biogeochemistry: Oahu,

Hawai'i. Aquat. Geochem. **15**: 547–570. doi:10.1007/s10498-009-9067-2

Jones, D. R., D. M. Karl, and E. A. Laws. 1996. Growth rates and production of heterotrophic bacteria and phytoplankton in the North Pacific subtropical gyre. Deep-Sea Res. I: Oceanogr. Res. Pap. **43**: 1567–1580. doi:10.1016/S0967-0637(96)00079-9

Karl, D. M., K. M. Björkman, M. J. Church, L. A. Fujieki, E. M. Grabowski, and R. M. Letelier. 2022. Temporal dynamics of total microbial biomass and particulate detritus at station ALOHA. Prog. Oceanogr. **205**: 102803. doi:10.1016/j.pocean.2022.102803

Lapointe, B. E., and B. J. Bedford. 2011. Stormwater nutrient inputs favor growth of non-native macroalgae (Rhodophyta) on O'ahu, Hawaiian islands. Harmful Algae **10**: 310–318. doi:10.1016/j.hal.2010.11.004

Laws, E. A., J. Hiraoka, M. Mura, B. Punu, T. Rust, S. Vink, and C. Yamamura. 1994. Impact of land runoff on water quality in an Hawaiian estuary. Mar. Environ. Res. **38**: 225–241. doi:10.1016/0141-1136(94)90009-4

Laws, E. A., D. Ziemann, and D. Schulman. 1999. Coastal water quality in Hawaii: The importance of buffer zones and dilution. Mar. Environ. Res. **48**: 1–21. doi:10.1016/S0141-1136(99)00029-X

Leichter, J. J., and S. J. Genovese. 2006. Intermittent upwelling and subsidized growth of the scleractinian coral *Madracis mirabilis* on the deep fore-reef slope of Discovery Bay, Jamaica. Mar. Ecol. Prog. Ser. **316**: 95–103. doi:10.3354/meps316095

Leichter, J. J., and others. 2013. Transport and retention processes on Moorea, French Polynesia. Oceanography **26**: 52–63. doi:10.5670/oceanog.2013.45

Li, Y., and others. 2019. Long-term trend of the tropical Pacific trade winds under global warming and its causes. J. Geophys. Res.: Oceans **124**: 2626–2640. doi:10.1029/2018JC014603

Liu, H., H. A. Nolla, and L. Campbell. 1997. *Prochlorococcus* growth rate and contribution to primary production in the equatorial and subtropical North Pacific Ocean. Aquat. Microb. Ecol. **12**: 39–47. doi:10.3354/ame012039

Mackey, K. R. M., A. Paytan, K. Caldeira, A. R. Grossman, D. Moran, M. McIlvin, and M. A. Saito. 2013. Effect of temperature on photosynthesis and growth in marine *Synechococcus* spp. Plant Physiol. **163**: 815–829. doi:10.1104/pp.113.221937

Malmstrom, R. R., A. Coe, G. C. Kettler, A. C. Martiny, J. Frias-Lopez, E. R. Zinser, and S. W. Chisholm. 2010. Temporal dynamics of *Prochlorococcus* ecotypes in the Atlantic and Pacific oceans. ISME J. **4**: 1252–1264. doi:10.1038/ismej.2010.60

McManus, M. A., J. C. Sevadjian, K. J. Benoit-Bird, O. M. Cheriton, A. H. V. Timmerman, and C. M. Waluk. 2012. Observations of thin layers in coastal Hawaiian waters. Estuaries Coasts **35**: 1119–1127. doi:10.1007/s12237-012-9497-8

Messié, M., A. Petrenko, A. M. Doglioli, E. Martinez, and S. Alvain. 2022. Basin-scale biogeochemical and ecological impacts of islands in the tropical Pacific Ocean. Nat. Geosci. **15**: 469–474. doi:10.1038/s41561-022-00957-8

Moore, L. R., A. F. Post, G. Rocap, and S. W. Chisholm. 2002. Utilization of different nitrogen sources by the marine cyanobacteria *Prochlorococcus* and *Synechococcus*. Limnol. Oceanogr. **47**: 989–996. doi:10.4319/lo.2002.47.4.0989

Moosdorf, N., T. Stieglitz, H. Waska, H. H. Dürr, and J. Hartmann. 2015. Submarine groundwater discharge from tropical islands: A review. Grundwasser **20**: 53–67. doi:10.1007/s00767-014-0275-3

Murphy, J., and J. P. Riley. 1962. A modified single solution method for the determination of phosphate in natural waters. Anal. Chim. Acta **27**: 31–36. doi:10.1016/S0003-2670(00)88444-5

Nelson, C. E., A. L. Alldredge, E. A. McCliment, L. A. Amaral-Zettler, and C. A. Carlson. 2011. Depleted dissolved organic carbon and distinct bacterial communities in the water column of a rapid-flushing coral reef ecosystem. ISME J. **5**: 1374–1387. doi:10.1038/ismej.2011.12

Nelson, C. E., L. Wegley Kelly, and A. F. Haas. 2023. Microbial interactions with dissolved organic matter are central to coral reef ecosystem function and resilience. Annu. Rev. Mar. Sci. **15**: 431–460. doi:10.1146/annurev-marine-042121-080917

Partensky, F., J. Blanchot, and D. Vaulot. 1999*a*. Differential distribution and ecology of *Prochlorococcus* and *Synechococcus* in oceanic waters: A review. Bull. Inst. Océanogr. **19**: 457–475.

Partensky, F., W. R. Hess, and D. Vaulot. 1999*b*. *Prochlorococcus*, a marine photosynthetic prokaryote of global significance. Microbiol. Mol. Biol. Rev. **63**: 106–127. doi:10.1128/MMBR.63.1.106-127.1999

Pasulka, A. L., M. R. Landry, D. A. A. Taniguchi, A. G. Taylor, and M. J. Church. 2013. Temporal dynamics of phytoplankton and heterotrophic protists at station ALOHA. Deep-Sea Res. II: Top. Stud. Oceanogr. **93**: 44–57. doi:10.1016/j.dsr2.2013.01.007

Petrenko, A. A. 1997. Detection and characterization of the sewage plume at Sand Island, Hawaii. Doctoral dissertation, University of Southern California. University of Southern California ProQuest Dissertations & Theses. https://www.proquest.com/dissertations-theses/detection-characterization-sewage-plume-at-sand/docview/304369984/se-2?accountid=147035

Reid, E. C., T. M. DeCarlo, A. L. Cohen, G. T. F. Wong, S. J. Lentz, A. Safaie, A. Hall, and K. A. Davis. 2019. Internal waves influence the thermal and nutrient environment on a shallow coral reef. Limnol. Oceanogr. **64**: 1949–1965. doi:10.1002/lno.11162

Rii, Y. M., D. M. Karl, and M. J. Church. 2016. Temporal and vertical variability in picophytoplankton primary productivity in the North Pacific Subtropical Gyre. Mar. Ecol. Prog. Ser. **562**: 1–18. doi:10.3354/meps11954

Rii, Y. M., R. R. Bidigare, and M. J. Church. 2018. Differential responses of eukaryotic phytoplankton to nitrogenous nutrients in the North Pacific Subtropical Gyre. Front. Mar. Sci. **5**: 92. doi:10.3389/fmars.2018.00092

Rissik, D., I. M. Suthers, and C. T. Taggart. 1997. Enhanced zooplankton abundance in the lee of an isolated reef in the south Coral Sea: The role of flow disturbance. J. Plankton Res. **19**: 1347–1368. doi:10.1093/plankt/19.9.1347

Ruhe, R. V., J. M. Williams, and E. L. Hill. 1965. Shorelines and submarine shelves, Oahu, Hawaii. J. Geol. **73**: 485–497. doi:10.1086/627079

Sander, F., and D. M. Steven. 1973. Organic productivity of inshore and offshore waters of Barbados: A study of the island mass effect. Bull. Mar. Sci. **23**: 771–792.

Schmoker, C., and S. Hernández-León. 2013. Stratification effects on the plankton of the subtropical Canary Current. Prog. Oceanogr. **119**: 24–31. doi:10.1016/j.pocean.2013.08.006

Seki, M. P., J. J. Polovina, R. E. Brainard, R. R. Bidigare, C. L. Leonard, and D. G. Foley. 2001. Biological enhancement at cyclonic eddies tracked with GOES thermal imagery in Hawaiian waters. Geophys. Res. Lett. **28**: 1583–1586. doi:10.1029/2000GL012439

Shiozaki, T., T. Kodama, and K. Furuya. 2014. Large-scale impact of the island mass effect through nitrogen fixation in the western South Pacific Ocean. Geophys. Res. Lett. **41**: 2907–2913. doi:10.1002/2014GL059835

Signorini, S. R., C. R. McClain, and Y. Dandonneau. 1999. Mixing and phytoplankton bloom in the wake of the Marquesas Islands. Geophys. Res. Lett. **26**: 3121–3124. doi:10.1029/1999GL010470

Šilović, T., H. Mihanović, M. Batistić, I. D. Radić, E. Hrustić, and M. Najdek. 2018. Picoplankton distribution influenced by thermohaline circulation in the southern Adriatic. Cont. Shelf Res. **155**: 21–33. doi:10.1016/j.csr.2018.01.007

Sohm, J. A., N. A. Ahlgren, Z. J. Thomson, C. Williams, J. W. Moffett, M. A. Saito, E. A. Webb, and G. Rocap. 2016. Co-occurring *Synechococcus* ecotypes occupy four major oceanic regimes defined by temperature, macronutrients and iron. ISME J. **10**: 333–345. doi:10.1038/ismej.2015.115

The State of Hawai'i Department of Health - Environmental Management Division. 2017. Report to the twenty-ninth legislature. State of Hawai'i—2018 Regular Session—Relating to Cesspools and Prioritization for Replacement.

Tucker, S., K. Freel, E. Monaghan, C. Sullivan, O. Ramfelt, Y. Rii, and M. Rappe. 2021. Spatial and temporal dynamics of SAR11 marine bacteria across a nearshore to offshore transect in the tropical Pacific Ocean. PeerJ **9**: e12274. doi:10.7717/peerj.12274

van den Engh, G. J., J. K. Doggett, A. W. Thompson, M. A. Doblin, C. N. G. Gimpel, and D. M. Karl. 2017. Dynamics of *Prochlorococcus* and *Synechococcus* at station ALOHA revealed through flow cytometry and high-resolution vertical sampling. Front. Mar. Sci. **4**: 359. doi:10.3389/fmars.2017.00359

van den Engh, G., O. Ulloa, and D. M. Karl. 2019. Monitoring microbial communities in the marine environment. Cytometry A **95**: 717–721. doi:10.1002/cyto.a.23763

Vedernikov, V. I., V. G. Bondur, M. E. Vinogradov, M. R. Landry, and M. N. Tsidilina. 2007. Anthropogenic influence on the planktonic community in the basin of Mamala Bay (Oahu Island, Hawaii) based on field and satellite data. Oceanology **47**: 221–237. doi:10.1134/S0001437007020099

Vollbrecht, C., P. Moehlenkamp, J. M. Gove, A. B. Neuheimer, and M. A. McManus. 2021. Long-term presence of the island mass effect at Rangiroa Atoll, French Polynesia. Front. Mar. Sci. **7**: 595294. doi:10.3389/fmars.2020.595294

Whittier, R. B., and A. I. El-Kadi. 2009. Human and environmental risk ranking of onsite sewage disposal systems for Oahu. https://scholarspace.manoa.hawaii.edu/handle/10125/50770

Whittier, R. B., and A. I. El-Kadi. 2014. Human and environmental risk ranking of onsite sewage disposal systems for the Hawaiian islands of Kauai, Molokai, Maui, and Hawaii. https://scholarspace.manoa.hawaii.edu/handle/10125/50771

Wolanski, E., and B. Delesalle. 1995. Upwelling by internal waves, Tahiti, French Polynesia. Cont. Shelf Res. **15**: 357–368. doi:10.1016/0278-4343(93)E0004-R

Xiang, B., B. Wang, J. Li, M. Zhao, and J.-Y. Lee. 2014. Understanding the Anthropogenically forced change of equatorial Pacific trade winds in coupled climate models. J. Clim. **27**: 8510–8526. doi:10.1175/JCLI-D-14-00115.1

Acknowledgments

Funding for this work was provided by the National Science Foundation (Hawai'i Ocean Time-series, OCE 1756517), the Office of Naval Research (Award number N0001414100054–Asia-Pacific Research Initiative for Sustainable Energy Systems [APRISES]), the State of Hawai'i, the Cooperative Institute for Marine and Atmospheric Research, Hawai'i, the Simons Foundation (SCOPE #721252 and #721264), and the Office of the Dean of the School of Ocean and Earth Science and Technology at University of Hawaii at Mānoa. We would like to thank the following people for assistance with fieldwork, instrumentation, and laboratory analysis: Sara Searson, Abby Bates, Mariam Moreno, Tucker Hull, Macarena Burgos Martin, Timothy Burrell, Ryan Tabata, Eric Shimabukuro, Dan Sadler, and Lance Fujieki. We thank the University of Hawai'i Marine Center, Parker Marine Corp., and Sea Engineering Inc. for vessel support.

Conflict of Interest

None declared.

Submitted 19 February 2024
Revised 17 July 2024
Accepted 19 September 2024

Associate editor: Katherina Petrou